Rheostat Re-Wired: Alternative Hypotheses for the Control of Thioredoxin Reduction Potentials

Kathryn D. Bewley[1¤a], Mishtu Dey[2,3¤b], Rebekah E. Bjork[2,3], Sangha Mitra[1], Sarah E. Chobot[1], Catherine L. Drennan[2,3,4], Sean J. Elliott[1]*

1 Department of Chemistry, Boston University, Boston, Massachusetts, United States of America, 2 Howard Hughes Medical Institute, Cambridge, Massachusetts, United States of America, 3 Department of Chemistry, Massachusetts Institute of Technology, Cambridge, Massachusetts, United States of America, 4 Department of Biology, Massachusetts Institute of Technology, Cambridge, Massachusetts, United States of America

¤a Current address: Department of Pharmaceutical Chemistry, University of California, San Francisco, San Francisco, California, United States of America
¤b Current address: Department of Chemistry, University of Iowa, Iowa City, Iowa, United States of America
* elliott@bu.edu

Data Availability Statement: All relevant data are within the paper and its Supporting Information files. X-ray structural data has been deposited in the Protein Data Bank repository and it bears the PDB ID 4XHM.pdb.

Abstract

Thioredoxins are small soluble proteins that contain a redox-active disulfide (CXXC). These disulfides are tuned to oxidizing or reducing potentials depending on the function of the thioredoxin within the cell. The mechanism by which the potential is tuned has been controversial, with two main hypotheses: first, that redox potential (E_m) is specifically governed by a molecular 'rheostat'—the XX amino acids, which influence the Cys pK_a values, and thereby, E_m; and second, the overall thermodynamics of protein folding stability regulates the potential. Here, we use protein film voltammetry (PFV) to measure the pH dependence of the redox potentials of a series of wild-type and mutant archaeal Trxs, PFV and glutathionine-equilibrium to corroborate the measured potentials, the fluorescence probe BADAN to measure pK_a values, guanidinium-based denaturation to measure protein unfolding, and X-ray crystallography to provide a structural basis for our functional analyses. We find that when these archaeal thioredoxins are probed directly using PFV, both the high and low potential thioredoxins display consistent 2H+:2e- coupling over a physiological pH range, in conflict with the conventional 'rheostat' model. Instead, folding measurements reveals an excellent correlation to reduction potentials, supporting the second hypothesis and revealing the molecular mechanism of reduction potential control in the ubiquitous Trx family.

Introduction

Thioredoxins and thioredoxin-like proteins (glutaredoxins and protein disulfide isomerases) are prevalent in nature and found throughout all kingdoms of life [1]. These disulfide/dithiol oxidoreductases function via their surface-exposed, redox-active disulfide bond. The cellular functions of these proteins vary, ranging from electron transfer in response to oxidative stress

to folding and refolding of proteins [1,2], while their varied functions are linked to the range of redox potentials spanned by the disulfide bond, nearly 300 mV [3,4]. The oxidative proteins such as DsbA and protein disulfide isomerase (PDI), aid in protein folding and have disulfide bonds with high redox potentials: reported values range from -89 mV to -124 mV [5–8] and -110 mV to -190 mV [9,10], respectively. Classical thioredoxins, such as Trx1 from *E. coli*, possess disulfide bonds of low redox potentials (-270 mV [11]), and have the ability to donate electrons to its partner proteins, one being ribonucleotide reductase [12].

One of the major questions that arises from studying thioredoxins, is why are the disulfide bonds of some members of this superfamily "oxidizing" and others "reducing"? What inherently governs the redox potential of the disulfide/dithiol redox couple? Understanding the molecular basis for these differences has been a topic of ongoing research for several decades [4–6,8,9,11,13–17] with most studies focusing on the *E. coli* proteins Trx1 and DsbA and their various mutants [4–6,11,13–16]. From the work presented to date, there are two prevalent hypotheses. The first is that the identity of the CXXC motif and the pK_a of the N-terminal cysteine thiol largely govern the redox potential of the disulfide bond, as a redox-based 'rheostat' [4,5,15]. In high potential DsbA, for example, the CXXC active site contains a histidine residue that has been proposed to hydrogen bond to the N-terminal cysteine in the reduced form of the protein [17], causing the pKa of that cysteine to shift to a lower value (~3.5) as has been proposed from spectroscopic measurements [15,16,18]. In contrast, lower potential (or, "reducing") Trxs lack a histidine in the CXXC motif and the spectroscopically observed cysteine thiol pK_a values are typical (~8) [19]. According to the pK_a model [4], the redox potential for the disulfide bonds found in both higher- and lower-potential Trx should be the same at infinitely low pH and then diverge in the physiological pH range due to the action of the redox linked pK_a values, resulting in the theoretical Pourbaix diagram shown in Fig 1 [4]. In particular, divergence would occur above pH 3.5 (the proposed unique pK_a of DsbA), as the unique
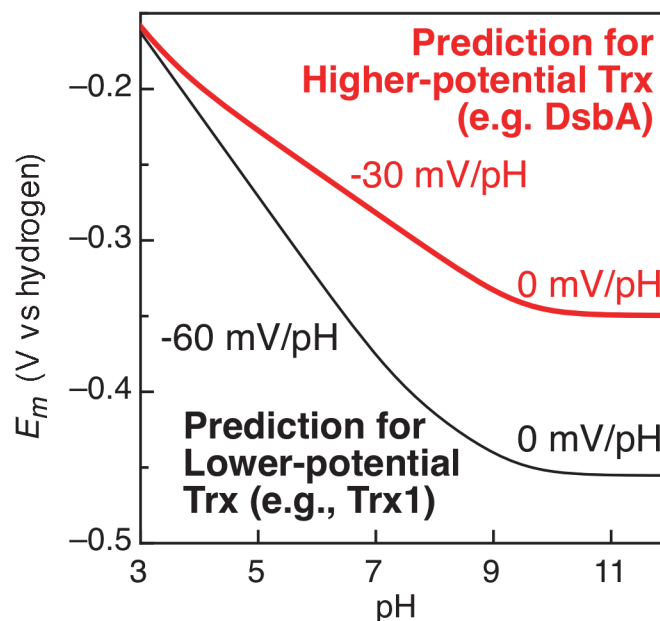
Fig 1. Theoretical and Experimental Pourbaix diagrams for DsbA and *E. coli* Trx1. Using the Nernst equation and the cysteine pKa values of DsbA (3.5) and Trx1 (7.1), the calculated dependence of redox potential on pH yields a difference in redox potential that is reflected in the different slopes within the Pourbaix diagram for higher-potential proteins (red) and lower-potential Trx proteins (black).

doi:10.1371/journal.pone.0122466.g001

pK_a associated with a higher-potential Trx redox couple yields a $1H^+:2e^-$ process (with a slope of -30 mV/pH). In contrast, the Trx proteins with a lower-potential disulfide bond follow a $2H^+:2e^-$ redox reaction [20] with slope of -59 mV/pH (25°C), due to the proposed similarity of the two Cys pK_a values. At high pH values (~9), the slope becomes flat (0 mV/pH), due to the fact that both cysteines would now be protonated. However, this calculated model is supported by experimental redox potential data collected only at physiological pH [4]. Additionally, the theory-based model relies on pK_a values determined by solution measurements, which themselves are not self-consistent [21]. (Indeed, the sparse data available on the pH dependencies of redox potentials for DsbA itself do not reveal a clear break in a Pourbaix diagram [5],[6], and suggest a slope of ~ -49 mV/pH, between the two limits of the pK_a-based model). Here for the first time we compare complete data sets of pH dependent redox potentials for high and low potential disulfide bond containing proteins using direct electrochemistry, and show that solution-based, spectroscopically determined pK_a measurements are not relevant for predicting redox potential.

The second hypothesis suggests that the overall fold of the protein dictates whether the oxidized or the reduced form is more stable thermodynamically, and thus influences the redox potential of the disulfide bond [5,6,22,23]. This view has been validated for DsbA, which is thought to undergo a global conformational change upon reduction where the oxidized state is thought to be 'tense' and the reduced state is more stable [6], and data consistent with this mechanism is available for *E. coli* Trx1, which is thought to only undergo local active site conformational changes [24]. In both wild-type and CXXC mutants of *E. coli* Trx1 [13], this second hypothesis is able to predict the redox potential found experimentally at pH 7. However, no series of Trx proteins has been examined in a side-by-side comparison of pK_a-based versus folding-based models.

In this paper we systematically test both hypotheses with a series of thioredoxins from *Archaeoglobus fulgidus (Af)* and *Thermoplasma acidophilum (Ta)*, which have been shown previously to possess disulfide bond redox potentials spanning -32 mV to -287 mV at pH 6 [3]. We have created various mutants installing hypothesized high-potential, histidine containing XX motifs into low-potential Trx protein folds. Our data include a thorough electrochemical study, cysteine pKa values, unfolding thermodynamic parameters, as well as crystallographic data showing that the archaeal Trx used for the basis of mutagenesis possesses a structure that is globally identical to other canonical Trx proteins. Together, these data show that the spectroscopically determined pK_a values of Cys residues in the archaeal proteins do not correlate with redox potentials, which is further corroborated by Pourbaix diagrams of both oxidizing and reducing-Trx proteins. In contrast, global unfolding energies yield an excellent correlation with reduction potential, suggesting that the CXXC 'rheostat' may well be governed more by folding than a specific pK_a-based 'wiring'.

Materials and Methods

Mutagenesis, Protein Expression and Purification

The expression and purification of *Af*Trx1, *Af*Trx3 [3] and *Ta*Trx [25] have been described previously. The *Af*Trx3 mutants were created using a mutagenesis kit (Stratagene) and the primers listed in **S1 Table**. The mutations were confirmed by DNA sequencing (Genewiz). The mutants were prepared in a similar manner to the wild-type protein. The empty pET-39b(+) vector (Novagen) was used as the source of DsbA. The pET-39b(+) vector was modified by adding a stop codon at the end of the C-terminal His-Tag. This modification allowed DsbA to be purified with a His-Tag, but removed 73 extraneous amino acids. DsbA was then expressed and purified using the same conditions as *Af*Trx3. The following two primers were used to

install the stop codon: forward 5'—C CAT CAC CAT CAC <u>TGA</u> GCG GGT CTG GTG—3'
and reverse 5'- CAC CAG ACC CGC <u>TCA</u> GTG ATG GTG ATG G—3'.

Protein Film Voltammetry

All protein film voltammetry experiments were conducted with a PGSTAT 12 potentiostat
(Ecochemie) housed in a Faraday cage. A three electrode configuration was used and the tem-
perature was controlled by using a circulator and a water-jacketed cell. The setup included a
platinum counter electrode, a calomel reference electrode, and a pyrolytic graphite edge (PGE)
working electrode. The PGE electrodes were sanded, polished with 1 μm alumina and sonicated
before use. Protein films were generated either by directly depositing a concentrated solution
of protein on the electrode, by soaking the electrode overnight in a dilute protein solution, or
by spin depositing. Spin deposition was achieved by rotating the electrode (200 rpm) in a dilute
solution of protein while applying either no voltage, or by scanning over a range of potentials.
Experiments were performed using argon purged buffer (20 mM NaAc, HEPES, MES, TAPS,
CHES, 50 mM NaCl) at 10°C. The raw data from each experiment was baseline subtracted and
analyzed using SOAS [26].

Glutathione Equilibrium Measurements

The redox equilibrium between glutathione and thioredoxin [5,9] was used to corroborate the
midpoint potential of AfTrx3, AfTrx3HP and AfTrx3PH, assuming a reference potential of the
$GSSG/(GSH)^2$ redox couple of -240 mV. Thioredoxin (1–2 μM) was equilibrated with 10 μM
oxidized glutathione (GSSG, Sigma Aldrich) and varying amounts of reduced glutathione (0–
200 mM, GSH, Sigma Aldrich) in argon purged buffer (100 mM sodium phosphate, pH 7 with
1 mM EDTA). The reactions were allowed to equilibrate in an MBraun glovebox overnight. A
fluorescence spectrum was taken for each sample (280 nm excitation, 300–400 nm emission,
25°C). The intensity at 345 nm was plot against $[GSH]^2/[GSSG]$ to obtain K_{eq}, which was used
to calculate the midpoint potential of thioredoxin as in References [5,9].

Cysteine Thiol pK$_a$ Determination

The method to determine the cysteine thiol pKa was adapted from Lewin et al [27,28]. Reduc-
tion of Trx was achieved with a 20-fold excess of DTT. After incubation for 30 minutes the ex-
cess DTT was removed with a PD-10 column. A mixed buffer system of 50 mM Tris HCl,
sodium citrate, K_2HPO_4 and CHES or 50 mM KCl, acetate, MES and Tris HCl was used for the
assay. Identical results were obtained from either buffer system. The fluorescent probe
BADAN [6-bromoacetyl-2-dimethylaminonaphthalene] (AnaSpec) was made fresh in DMF
every 45 minutes, as the intrinsic fluorescence intensity decreased after this amount of time.
Reduced Trx (0.25 μM) was allowed to equilibrate with buffer of various pH values at 23°C. Ki-
netic traces were then obtained by adding BADAN (3.25 μM), and recording the fluorescence
emission at 536 nm (excitation wavelength 387 nm) using a SpectraMax M2 plate reader (Mo-
lecular Devices). The initial rate (linear slope) of the reaction was obtained and was plot against
pH. It was found that similar results could be obtained by plotting the initial fluorescence in-
tensity (when an equal amount of BADAN and Trx were used) verses pH.

Protein Unfolding/Refolding Fluorescence

A stock solution of 8 M guanidine hydrochloride (Sigma Aldrich), pH 7 was used in the un-
folding experiments. By using varying amounts of guanidine and buffer (10 mM HEPES,
150 mM NaCl, pH 7) the protein (final concentration of 5 μM) was equilibrated in 0 M—7 M

guanidine HCl (GdnHCl) for 24–72 hours at room temperature. Oxidized unfolding experiments were performed with air-oxidized protein. For the reduced unfolding experiments, protein samples were pre-reduced with dithiothreitol (DTT), and a final concentration of 1 mM DTT was added to each protein/guanidine solution to keep the protein in its reduced state. The reduced samples were also prepared and allowed to equilibrate an MBraun glovebox.

A Horiba Jobin Yvon FluoroMax 3 fluorimeter was used to collect the fluorescence unfolding data, using a 5 mm x 5 mm path length quartz cuvette, thermostated at 25°C with a water circulator. An excitation wavelength of 280 nm was used with a 2 mm slit width, and emission spectra were collected at 300–450 nm (3 mm slit width). Data was taken every 1 nm with a 0.5 sec integration time.

Protein Crystallization and X-Ray Crystallography

*Af*Trx3HP crystals were grown at room temperature by incubating 1.0 µl of 20 mg/ml protein solution (in 10 mM HEPES pH 7.0 and 20 mM NaCl) and 1.0 µl of precipitant solution containing 60% Tacsimate, pH 7.0 using sitting drop method. Rod-shaped crystals of approximately 100–150 µm grew in 3–4 days. Crystals were cryo-protected in precipitant solution containing 10% glycerol by soaking for 2–5 minutes before flash-freezing in liquid nitrogen.

X-ray diffraction data were collected at 100 K in-house using a Rigaku R-AXIS IV IP detector. Data were subsequently integrated and scaled in DENZO and SCALEPACK respectively [29]. The crystals belong to the orthorhombic space group $P2_12_12_1$, with two thioredoxin molecules per asymmetric unit. The structure was solved to 1.95 Å resolution by molecular replacement using *Staphylococcus aureus* thioredoxin (PDB ID 2O7K) as a search model. Water molecules were removed from the initial search model used for molecular replacement in PHASER [30] that gave a Z-score of 12.0, suggesting a correct solution. Using a chainsaw model of the initial solution, correct residues and side chains were introduced in COOT [31] and a restrained refinement in REFMAC [32] from the CCP4 Program Suite [33] resulted in R_{free} of 35.0% and R_{work} of 29.9%. Subsequent rounds of refinement were carried out in CNS [34], which included iterative rounds of energy minimization, B-factor refinement, simulated annealing. Final refinement was carried out in PHENIX [35], which allowed Cys 59 and Cys 62 to be refined as a 50:50 mixture of oxidized and reduced disulfide bonds. Model building was performed in COOT using SigmaA weighted $2F_o$-F_c and F_o-F_c maps. Water molecules were included automatically using COOT and were manually checked against $2F_o$-F_c and F_o-F_c electron density maps. The structure was analyzed using $2F_o$-F_c composite omit maps and Ramachandran geometries were analyzed with PROCHECK [36]. The final model contains residues 25–134 (of 134) for chain A and residues 26–134 (of 134) for chain B (Protein Data Bank (PDB) ID 4XHM.pdb).

Results

Re-wiring the 'rheostat': *Af*Trx is structurally homologous to canonical Trx

Mutants of *Af*Trx3 that altered the identity of the residues between the two active site cysteines were generated (**Table 1**) to test the CXXC redox rheostat model, where hydrogen bonding between the N-terminal Cys and a histidine within this active site is proposed to occur [17]. We therefore created mutants of the wild-type CMPC sequence, substituting histidine, as well as lysine at the XX positions. As the names imply, the mutant *Af*Trx3HP has the active site sequence CHPC; *Af*Trx3PH has the sequence CPHC, and *Af*Trx3KP has the sequence CKPC (Table 1). These were successfully expressed and purified.

Table 1. Electrochemical potentials and Cys pKa values of thioredoxins.

| Trx	CXXC	E_m (mV)	δ (mV)	Spectroscopic Cys pK_a value
TaTrx	CHPC	-64[a]	60	6.5 ± 0.1
AfTrx1	CPHC	-32[b]	62[b]	6.8 ± 0.1
AfTrx3	CMPC	-287[b]	56[b]	7.0 ± 0.1
AfTrx3HP	CHPC	-291[a]	56	7.0 ± 0.1
AfTrx3PH	CPHC	-221[a]	60	4.2 ±0.2, 7.3 ± 0.3
AfTrx3KP	CKPC	-315[a]	46	7.2 ± 0.1
DsbA	CPHC	-89[c],-124[d]	—	3.1 ± 0.2

[a]determined by PFV at pH 7.0

[b]from Ref [3]

[c]from reference [5]

[d] from Ref [6–8].

doi:10.1371/journal.pone.0122466.t001

To ensure that AfTrx3 is a representative Trx, the crystal structure of AfTrx3HP was solved to 1.95 Å resolution (see S2 Table). The AfTrx3HP mutant crystallized better than wild-type and thus was used to provide a structural depiction of this archaeal protein. The structure consists of two molecules in the asymmetric unit (a.s.u), where both structures are complete except for the first 25–26 residues at N-termini, which are disordered. AfTrx3HP shares the classic Trx fold, consisting of a central core of five β-strands enclosed by four α-helices (Fig 2A). The active site loop is found at the end of a α-helix on the surface of the protein where it can interact with its partner proteins to catalyze disulfide exchange. In both structures in the a.s.u., the Cys 59-Cys 62 disulfide bond appears to be a ~50:50 mixture of oxidized and reduced conformations (Fig 2B and 2C). Comparison with E. coli Trx in the region of the active site shows that the only major difference is in the sequence of the CXXC loop itself. In particular, the difference is due to the substitution of His (60 in this A. fulgidus mutant) with Gly (33 in E. coli). All other residues near the active site disulfide are conserved (see below).
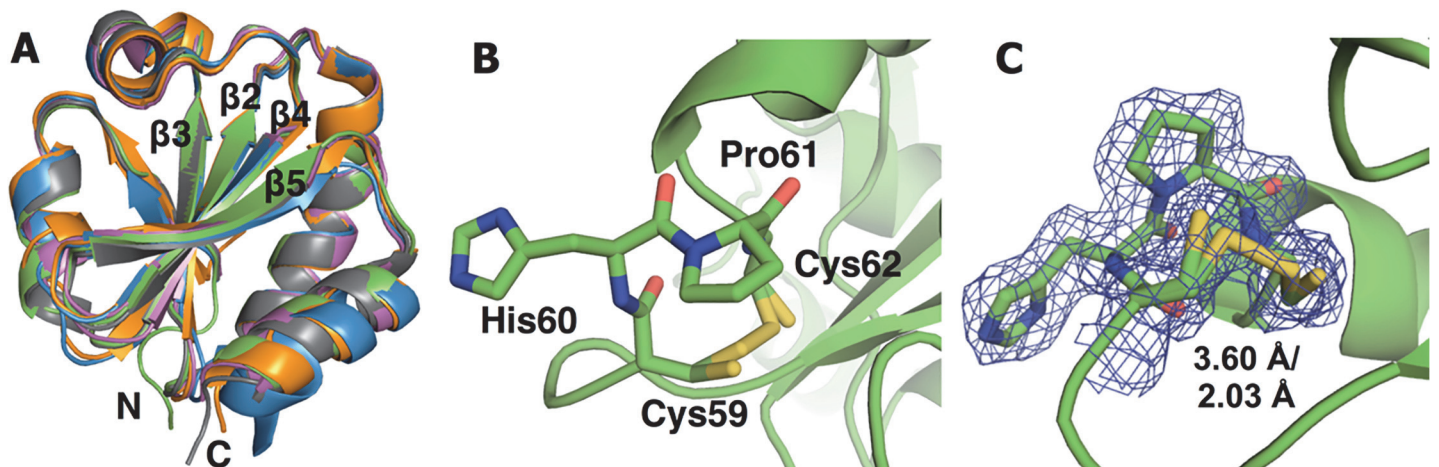
Fig 2. Structural analysis of thioredoxins. (A) Structural comparison of AfTrx3HP (green) with thioredoxins from S. aureus (magenta), E. coli (orange), T. thermophilus (grey), and A. acidocaldarius (sky blue) with r.m.s.d's of 0.66 Å, 0.68 Å, 0.40 Å, and 0.70 Å respectively. (B) AfTrx3HP cysteine loop with the active site CHPC motif. (C) $2F_o$-F_c α_{omit} density (contoured at 1 σ) is consistent with 50:50 mixture of oxidized (2.03 Å distance) and reduced (3.60 Å distance) conformations of the Cys 59-Cys 62 disulfide. The main chain and side chain residues are shown as sticks with oxygens in red, nitrogens in blue, sulfurs in yellow, and carbons are in green similar to protein backbone.

doi:10.1371/journal.pone.0122466.g002
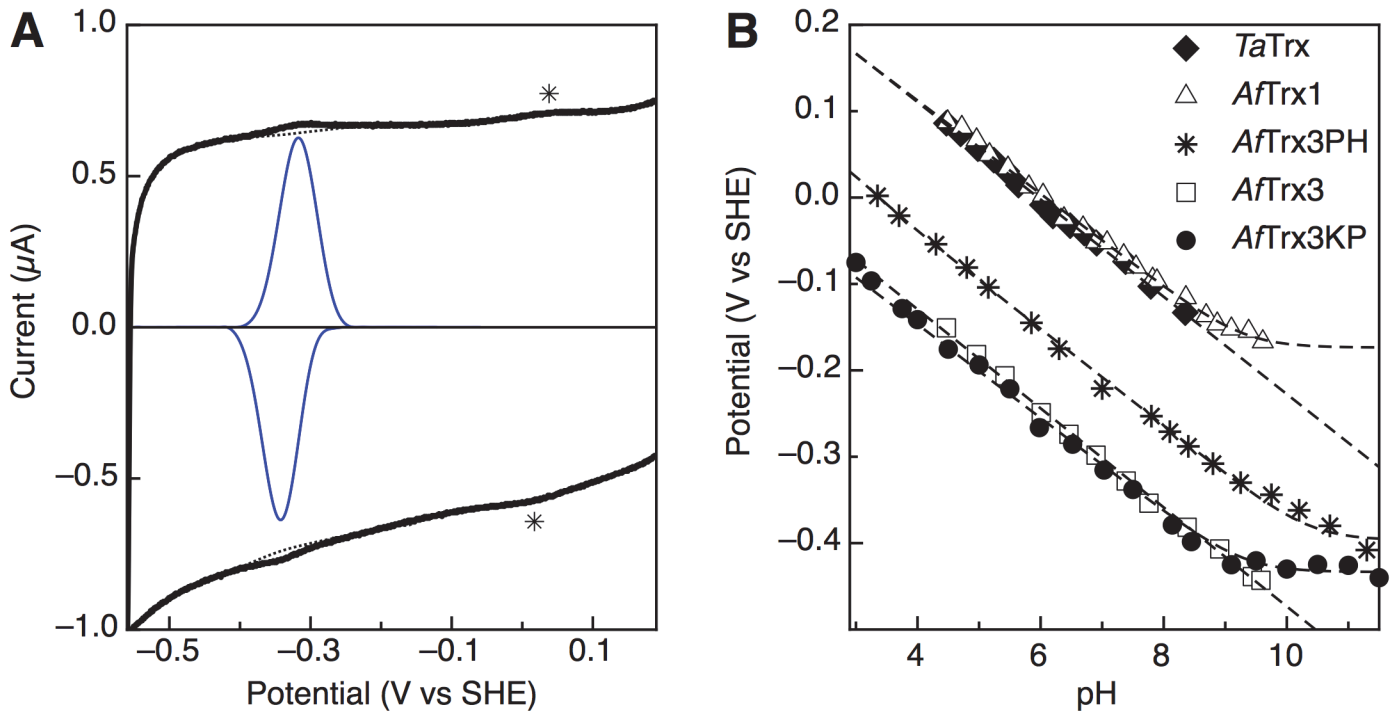
Fig 3. Direct electrochemistry of archaeal Trx proteins. (A) An example of direct PFV analysis of Trx3s proteins. Background capacitance of the blank electrode (dashed line) can be subtracted from the raw data (heavy) to reveal highly cooperative 2-electron redox couples (solid line), with a surface feature of graphite electrodes indicated as *. (B) Pourbaix diagrams for thioredoxins *Ta*Trx (diamonds), *Af*Trx1(triangles), *Af*Trx3PH (asterisks), *Af*Trx3 (squares), and *Af*Trx3KP(bullets).

doi:10.1371/journal.pone.0122466.g003

Protein Film Voltammetry Reveals 2H⁺:2e⁻ Stoichiometries

To assess the possible role of redox-linked pK_a values in distinguishing Trx disulfide bonds of varying potential, we conducted protein film voltammetry (PFV) studies of the Trx proteins and mutants of *Af* Trx3. Direct electrochemistry of these proteins allows for the precise evaluation of the redox couple of the disulfide bond itself through a cyclic voltammetry experiment of an immobilized protein sub-monolayer (**Fig 3A**). This approach allows for the facile determination of the pH dependence of E_m, plotted as a Pourbaix diagram (**Fig 3B**) that allows for comparison of novel Trx proteins studied here with our prior results for *Af* Trx3 [3].

The Trx proteins studied here have a range of E_m values at pH 7, which is loosely correlated to the identity of the variable residues in the CXXC motif (**Table 1**), where the uncertainty is 2–3 mV for each Trx examined. *Ta*Trx displays a high potential (similar to *Af*Trx1) and both possess a His residue in the variable region of the CXXC motif. However, the *Af*Trx3PH mutant, which also has a His residue in the CXXC motif, has a midpoint potential that is only slightly higher than wild-type *Af*Trx3, which has no His. At neutral pH the other mutants that have installed alternative residues in the CXXC motif of the *Af*Trx3 active site were found to be similar to wild-type (*e.g.*, *Af*Trx3HP and *Af*Trx3KP proteins). Regardless of their redox potential at pH 7, Pourbiax diagrams reveal parallel slopes of approximately -56 mV / pH unit, the theoretical value for a 2H⁺:2e⁻ coupled process over the entirety of the pH range studied. Critically, there does not appear to be a pK_a value observed between pH values of 3 and 9, as predicted by the supposition that a high-potential disulfide bond results from a uniquely low Cys pK_a in the Trx 'rheostat'. Only *Af*Trx1, *Af*Trx3PH and *Af*Trx3KP show pK_a values that can be determined from electrochemistry: 9.1, 10.4, and 9.2, respectively. Although it is clear that the

pK_a values must be nearly identical for both Cys residues for *Ta*Trx and *Af*Trx3, the precise pK_a values could not be measured as the electrode:protein interaction was not stable at high pH values.

Analysis of the voltammetric peak width at half-height reveals the number of electrons giving rise to that signal. Although the theoretical values of 1- versus 2-electron processes are 86 mV and 43 mV, respectively, we have previously shown that the peak widths of thermophilic thioredoxins on graphite electrodes are artificially broadened, to ~60 mV at the low temperature of 10°C [3], which is used to ensure stability of the protein film over multiple experiments. Consistent with our prior findings of disulfide-bond electrochemistry, these Trxs show peak widths around 60 mV at 10°C (**Table 1**), indicating 2-electron processes.

To corroborate the shifts in redox potential for the *Af*Trx3 mutants, glutathione (GSH/GSSG) redox titrations were used at pH 7. In all cases, the titration results agreed with PFV, though the measured potentials were slightly shifted to more oxidizing potentials: The variations range from 9 mV more positive (for *Af*Trx3PH, where the E_m value measured by PFV was -221 mV, compared to -212 mV from titrations) to 20 mV more positive (for *Af*Trx3, where E_m was -287 mV by PFV, and measured as -267 by titration).

## Higher-potential Disulfide Bonds Need Not Have Low Cys pK_a Values

To support the finding by PFV that pK_a values are not correlated to the potentials of the Trx disulfide bonds studied here, we employed a spectroscopic method to verify the Cys pK_a values of the CXXC motif. The fluorescence probe BADAN was used to selectively label the thiolates of the CXXC [27] (**Fig 4**). Instead of monitoring the 240 nm optical absorbance of the thiolate itself [16], which we found to be unreliable, we chose the method developed by Lewin *et al.* [27,28] for its reproducibility. For these Trx proteins we monitored both the rate of the reaction with BADAN over time (**Fig 4A and 4B**), as well as observed the initial fluorescence intensity of a reaction where equal amounts of protein and BADAN were mixed. Nearly identical results were found with each variation. Plotting either the initial velocity of the BADAN reaction, or the initial fluorescence intensity after mixing, as a function of pH, results in resolution of the spectroscopically determined pK_a values of the active site Cys residue(s), where DsbA is used as positive control (**Fig 4C**). The results are displayed in **Table 1**. Most of the Trx proteins were found to have a single pK_a of around 7, similar to *E. coli* Trx1. Importantly, the higher-potential Trx proteins (*Ta*Trx and *Af*Trx1) did not have low pK_a values. Interestingly, *Af*Trx3PH was found to have two pK_a values, one of which (4.2) has been shifted significantly (**Fig 4E**).

The Energetics of Unfolding Resolves the Determinants of Redox Potential

An alternate view of the control of disulfide reduction potentials has been ascribed to the difference in global folding stability of the Trx proteins themselves. In such a model, the redox potential of the natively folded protein can be calculated on the basis of a free-energy for the native redox reaction (ΔG_N), which results from consideration of a thermodynamic square scheme (**Fig 5**). In such a model ΔG_N is derived from measurements of the folding/unfolding energetics of both the oxidized and reduced forms of each protein (which provide values of $\Delta G_{Stab(Ox)}$ and $\Delta G_{Stab(Red)}$) and a reference value of the redox potential of an "unfolded" protein-based disulfide bond (ΔG_U).

Folding and unfolding experiments were performed on the collection of *Af*Trx3 and the *Af*Trx3 mutants, and in each case the Trx revealed reversible, two-state unfolding (**Fig 6**). The oxidized forms of *Af*Trx3, *Af*Trx3HP and *Af*Trx3KP are more stable than the reduced forms, as determined by required concentrations of denaturant required to unfold the protein ($D_{1/2}$)
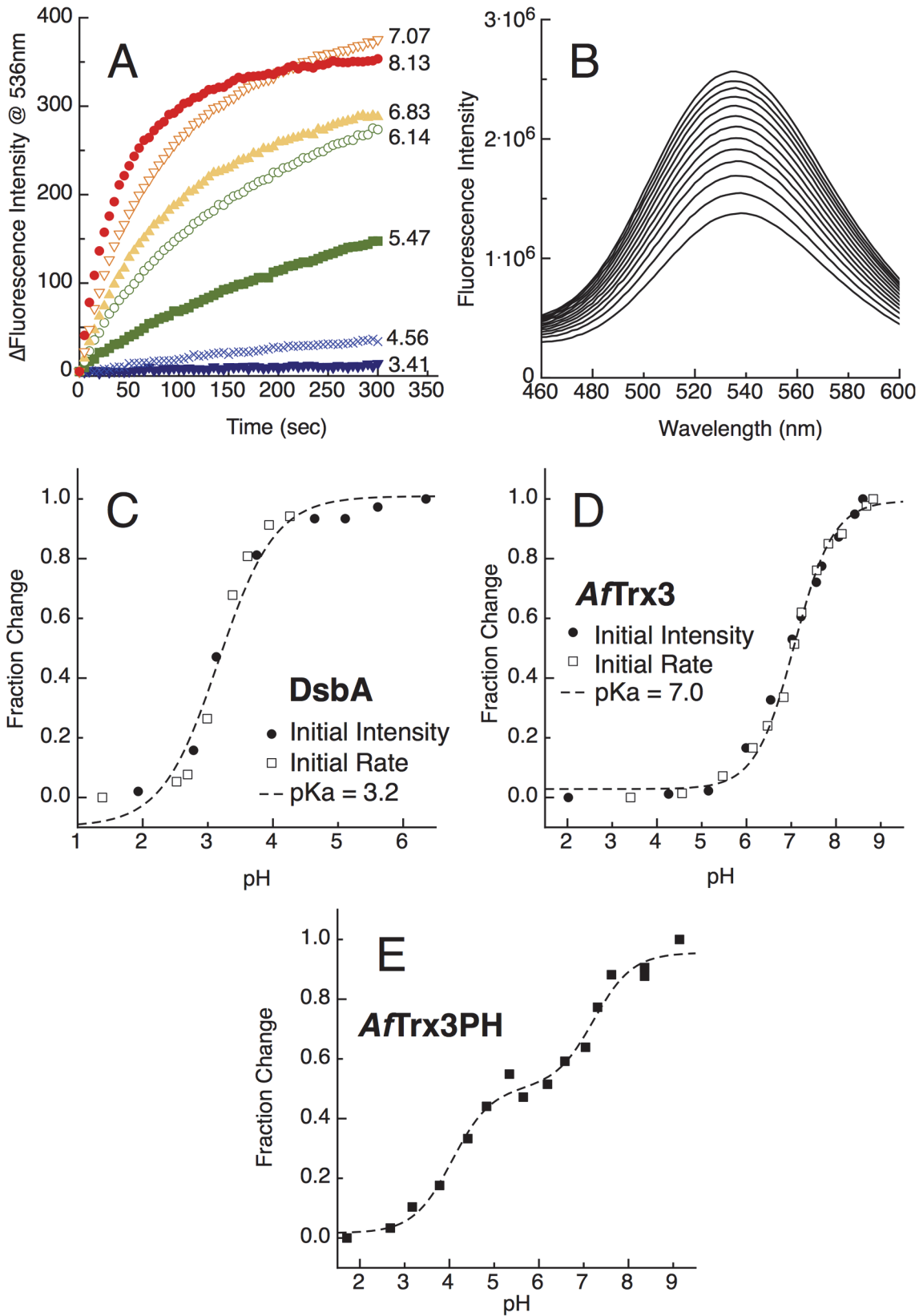
Fig 4. Cysteine thiol pKa determination. (A) The change in fluorescence intensity of *Af*Trx3 (0.25 µM) and BADAN (3.25 µM) over time in a variety of pH values. (B) The emission spectra of *Af*Trx3 (0.25 µM) and BADAN (3.25 µM) over time at pH 7.5, 387 nm excitation. Both the initial rates of the reaction, and the fluorescence intensity of equimolar protein and BADAN are then monitored as a function of pH to determine the spectroscopically monitored pKa values for: (C) DsbA, (D) *Af*Trx3, and (E) *Af*Trx3PH.

([Table 2](#)). Having a more stable oxidized form is a trait of a reducing thioredoxin [6,37,38], and these results correlate to their midpoint potentials. For example, *Af*Trx3PH, has oxidized and reduced forms that are nearly equally stable, indicating the redox potential is higher than wild-type *Af*Trx3 (as found by PFV analysis). Free energies of stabilization at zero denaturant concentration (ΔG_{Stab}), for the oxidized and reduced proteins were then calculated by extrapolating a linear dependence of free energy versus guanidinium concentration (see **S1 Methods** for equations [39,40]). Using these free energies and the square scheme of **Fig 5**, ΔG_N (and the corresponding redox potentials) can be found, though doing so requires a value of ΔG_U. Here, we have used glutathione (E_m -240 mV[41]) as a reference point for an "unfolded" protein reduction potential [5,8,9] where ΔG_U is 7.9 kJ/mol [6]. Fundamentally this value is the redox potential of a disulfide bond in a chemical context similar to a peptide, and should be protein independent [8]. Indeed, using DsbA as a control, our results match what has been previously reported [6]. However, we note that through this method, we lack a genuine standard potential for an unfolded disulfide-bearing protein. Regardless, application of the thermodynamic square scheme allows for the generation of calculated E_m values for each Trx protein at pH 7, and **Table 2** provides a comparison of the thermodynamically calculated redox potentials with the experimental potentials listed in [Table 1](#).

*Af*Trx1 and *Ta*Trx folding experiments are complicated by the fact that these proteins likely contain one (*Af*Trx1) or two (*Ta*Trx) internal, structural disulfides (**S1 Fig**), yet only a single redox active disulfide detected by PFV. We believe the unfolding curves for the reduced versions of these proteins (*e.g.* see the black data for *Ta*Trx in **Fig 6A**) are shifted to lower guanidine concentrations due to the reduction of both the redox disulfide and the internal disulfides. The oxidized unfolding traces of *Ta*Trx do not show a clean two-state transition (orange data), including biphasic behavior as well as some degree of hysteresis in the refolding, which may be due to inter- or intra-protein disulfide bond exchange. Due to these complications, we focused
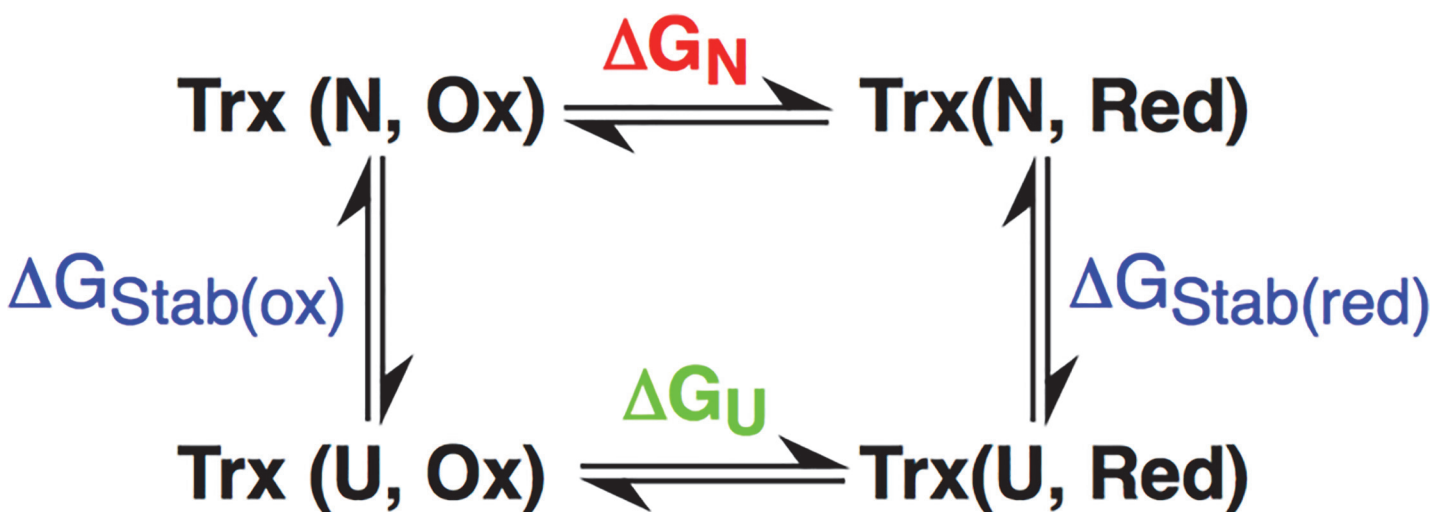
Fig 5. Thermodynamic square used to predict redox potential of disulfide bond containing proteins. Here, ΔG_N is determined and then correlated to a value of E_m.
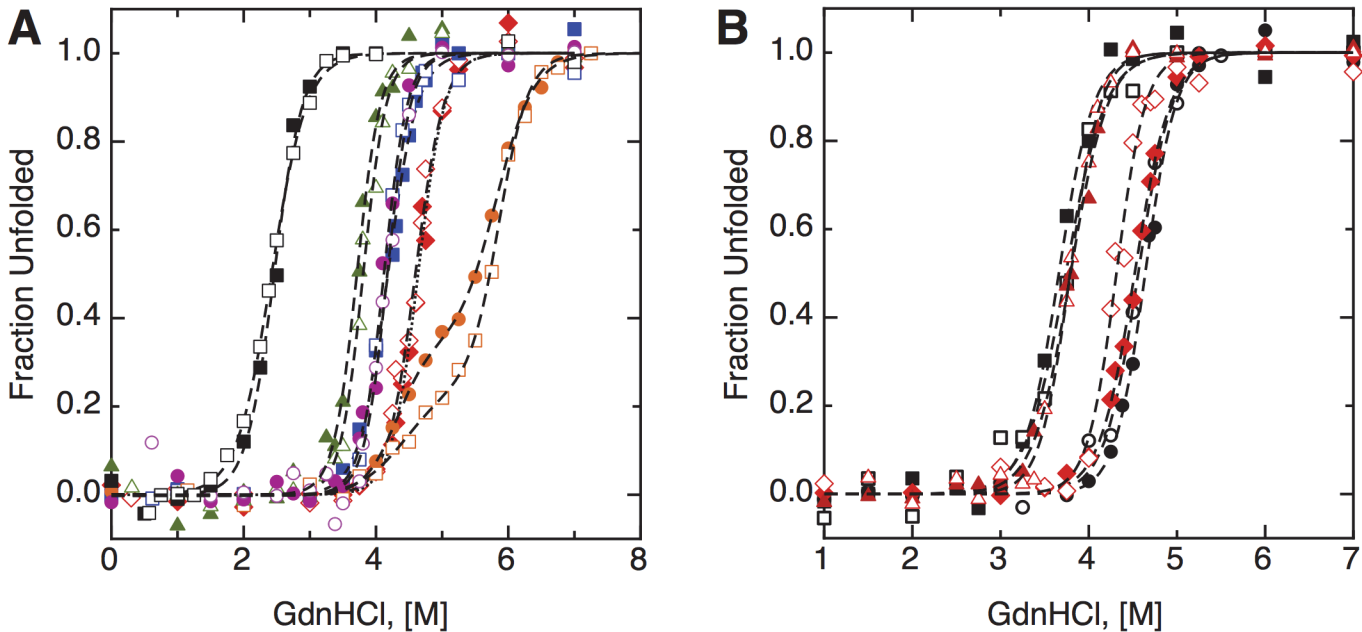
Fig 6. Fluorescence unfolding/refolding plots. The fraction of the protein that is unfolded is depicted versus the concentration of guanidine HCl in solution (A) closed symbols are unfolding and open symbols are refolding for *Af*Trx3/oxidized (red), *Af*Trx3PH/oxidized (blue), *Ta*Trx/oxidized (orange), *Af*Trx3/reduced (green), *Af*Trx3PH/reduced (pink), *Ta*Trx/reduced (black). For the sake of clarity, (B) shows similar curves for *Af*Trx3KP oxidized (black circles) and reduced (black squares), and *Af*Trx3HP oxidized (red diamonds) and reduced proteins (red triangles).

doi:10.1371/journal.pone.0122466.g006

on *Af*Trx3 and its mutants for the unfolding model studies. *Af*Trx3, *E. coli* Trx1 and DsbA each contain only the two cysteines that form the redox active disulfide, and follow a two-state unfolding. And their collective analyses clarify the potential impact of folding-based stabilization of disulfide bond redox potentials.

Discussion

Here we report the first example of a full Pourbaix diagram for disulfide bounds of high potential found in thioredoxin proteins (*Af*Trx1 and *Ta*Trx). Through the examination of these and other archaeal Trx proteins, we have been able to specifically interrogate the pK_a-governed model of control of disulfide-bond redox potentials. In all cases studied here, Pourbaix analysis (measuring complete pH-dependence of the potential) indicates a continuous slope of ~-60 mV/pH from low pH to above pH 9, suggesting $2H^+:2e^-$ coupling. The electrochemical data themselves reveal that the redox couples must be for $2e^-$ processes due to the narrow peak-width at half-height values ([Table 1]). Complete descriptions of proton-coupled redox processes of disulfide bond-bearing proteins has been rare, particularly when considering the ubiquity

Table 2. Fluorescence unfolding/refolding thermodynamics and calculated midpoint potentials.

| Trx	CXXC	D$_{1/2}$ (Oxidized)	ΔG$_{Stab(Ox)}$	D$_{1/2}$ (Reduced)	ΔG$_{Stab(Red)}$	Calculated E_m
*Af*Trx3	CMPC	4.6 ± 0.2M	59 ± 3 kJ/mol	3.8 ± 0.1M	50 ± 6 kJ/mol	-245 mV
*Af*Trx3HP	CHPC	4.5 ± 0.1M	53 ± 2 kJ/mol	3.7 ± 0.1M	44 ± 2 kJ/mol	-246 mV
*Af*Trx3PH	CPHC	4.2 ± 0.1M	57 ± 6 kJ/mol	4.1 ± 0.1M	58 ± 2 kJ/mol	-194 mV
*Af*Trx3KP	CKPC	4.6 ± 0.2M	59 ± 1 kJ/mol	3.8 ± 0.1M	47 ± 5 kJ/mol	-261 mV
DsbA	CPHC	2.0 M	40 kJ/mol	2.1M	56 kJ/mol	-116 mV

doi:10.1371/journal.pone.0122466.t002

of the Trx superfamily. And as noted above, previous work by Wunderlich and Glockshuber indicated with a small number of data-points that DsbA displays a pH-dependent potential of -49 mV/pH unit [5]. Although DsbA itself was found to be inactive to electrochemical analysis (due to insufficient adsorption at the electrodes utilized), here we have been able to use the rapid facility of PFV to our advantage, to produce more complete Pourbaix diagrams, with higher numbers of data points for other Trxs. Our approach allows us to fully describe the redox chemistry of higher-potential disulfide bonds found in the Trx family (*Af*Trx1 and *Ta*Trx), revealing that redox-linked protonations for the high-potential Trx proteins occur with pK$_a$ values typical for Cys residues (**Fig 3B**), in disagreement with the pK$_a$-governed model depicted in **Fig 1** [4].

In the pK$_a$-governed redox model, the identity of the variable residues (and the inclusion of a His) in the CXXC is thought to impact the redox potential. Experimentally we have examined this issue with the *Af*Trx3 protein, using it as a scaffold to produce *Af*Trx3HP (CHPC) and *Af*Trx3PH (CPHC) mutants. The *Af*Trx3HP mutant behaves similarly to the wild-type (CMPC) protein: The midpoint potential is low, and the unfolding/refolding data does not show a major deviation from wild-type. *Af*Trx3PH, however, is different from wild-type. This mutant has a +66 mV shift in the redox potential, but again reveals Pourbaix diagrams devoid of features indicating a uniquely low pK$_a$ associated with redox chemistry. The unfolding/re-folding data for *Af*Trx3PH also differs from wild-type, as both the oxidized and reduced forms are equally stable. Notably, using the spectroscopic probe BADAN, we determined the apparent pK$_a$ for Cys residues. By the spectroscopic approach, the placement of His in the second variable position (like DsbA) does result in a shifted pK$_a$ value (4.2, Fig 4E). Yet these values do not correlate to redox-linked pK$_a$ values as determined by direct electrochemistry, nor do they correlate with redox potentials. Thus, we find that the spectroscopically reported values may result from aggregate phenomena that are not linked to redox chemistry directly (as is portrayed by a Pourbaix diagram).

In addition to the specific role in modulation of Cys pK$_a$ values, hydrogen-bonding interactions (particularly with the N-terminal Cys residue) have been implicated in the activity of Trx proteins by Berndt and co-workers [42]. Intriguingly, here there are no apparent hydrogen-bonding interactions at work in the Trx active site, as observed for the *Af*Trx3HP structure. Indeed the disulfide is in a hydrophobic environment, blocked from direct contact with solvent by residues Trp 58, Pro 61, Ile 102, Pro 103. The only potential hydrogen bond is from the N-term Cys to the carbonyl of Ile 102 (3.18 Å). There are no H-bonding networks that would be expected to alter the pKa of either Cys. In fact, both cysteine side chains are beautifully sandwiched by hydrophobic residues on all sides.

Might there be any role for histidine in the determination of the redox potentials of Trx-based disulfide bonds? Inspection of the structure of the *Af*Trx3HP CHPC motif (**Fig 2**, inset) shows M60H is oriented out into solution, and is neither able to interact with the cysteine in the active site nor is it able to provide any stabilizing hydrogen bonding interactions with any part of the protein fold. Thus, our structure is consistent with the data presented above and helps to explain why the M60H mutation has no influence on either the redox or folding properties of *Af*Trx; this histidine sidechain is making no contacts. Although a structure of *Ta*Trx is not available, we predict that the histidine of the CHPC motif will also point out into solution based on the *Af*Trx3HP structure, which is the first of a Trx with a CHPC motif. Therefore, it seems unlikely that the histidine of the CHPC motif will be at all responsible for the high redox potential of *Ta*Trx. Although having a histidine at position 2 does not appear to have an influence on the redox properties, we also considered the relative importance of histidine at position 3. *Af*Trx3PH places histidine at position 3, with a sequence motif identical to DsbA (CPHC), yet the redox properties are more similar to wild-type *Af*Trx3 (-221 mV and -278 mV,
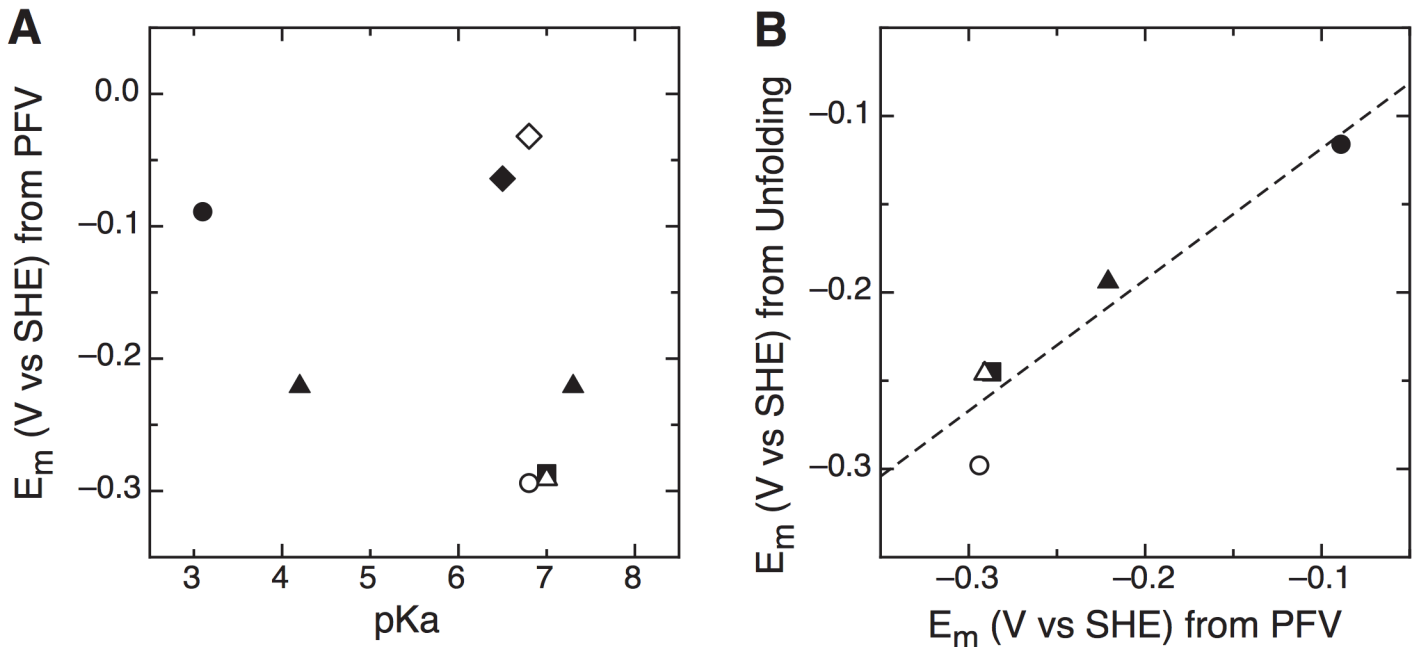
Fig 7. Correlations (and lack thereof) between redox potentials and other factors. (A) The pK$_a$-governed model cannot resolve a prediction of midpoint potential (*Ta*Trx (closed diamond), *Af*Trx1 (closed diamond), *Af*Trx3 (closed square), *Af*Trx3HP (open triangle), *Af*Trx3PH (closed triangle), *Af*Trx3KP (open circle), DsbA (closed circle)). (B) Global folding energies, used to calculate an E_m value correlate with potentials directly determined by PFV (*Af*Trx3 (closed square), *Af*Trx3HP (open triangle), *Af*Trx3PH (closed triangle), *Af*Trx3KP (open circle), DsbA (closed circle)).

doi:10.1371/journal.pone.0122466.g007

respectively) than there are to DsbA (-89, -124 mV), even though one pK$_a$ is observed spectroscopically at 4.2, and without structural evidence, we can only presume that the His present in *Af*Trx3PH could engage in hydrogen-bonding interactions with one or both of the redox-active cysteines. Again, the spectroscopic determinations of the Cys pK$_a$s do not correlate with the direct observation of redox-linkage observed in a Pourbaix diagram. Here we can conclude that in terms of redox-reactivity, the cysteines of the Trx proteins considered here are more like typical Cys side-chains, while the fluorescence-detected pK$_a$ values likely report on aggregated phenomena that is not tied to redox chemistry (and aside from the *Af*Trx3PH protein, may report on the composite pK$_a$s of both Cys residues). Considering all of the data in **Table 1**, there seems to be little correlation between CXHC proteins and potential, but perhaps the greater role in tuning redox potential is due placement of the proline residue, suggesting that overall or local folding traits more profoundly impact the redox potential.

Overall our data show that the solution-based pK$_a$ values do not govern the redox properties displayed by the Trx disulfide bonds. In solution, the pK$_a$ values of the free thiolates can only be measured when the protein is already reduced. These solution assays do not directly probe what the protonation state is *while* the reduction is occurring, in contrast to PFV. Thus, while the spectroscopically determined pK$_a$ values appear to be somewhat dependent on the nature of the CXXC motif, they do not correlated with the redox event that reduces the disulfide (**Fig 7A**). Aside from the pK$_a$ contribution (or lack thereof) our data show that the overall folding thermodynamics, when two-state folding can be applied, does quantitatively predict redox reactivity (**Fig 4** and **Table 2**). Whether or not this relationship is causal, cannot be determined at this time, yet it is clear that there is a correlation (**Fig 7B**). Structurally, *Af*Trx3, *Ec*Trx and others are similar, even if their CXXC differs, suggesting once again that the pK$_a$ alone is not driving the midpoint potential, and therefore reactivity. Given the roles that Trx paralogs and

Trx domains play in protein:protein redox reactions, a long-term ramification of this work is that intermolecular interactions may further modulate protein structure to tune the redox characteristics and reactivity of Trx disulfide bonds. We note as well that the thermodynamic potential alone may not govern the reactivity of any disulfide bond, particularly *in vivo*. For example, *E. coli* glutaredoxin 1 has a higher potential disulfide bond (-233 mV) than the principle Trx protein (-270 mV) [8], yet the differences in K_m for these proteins results in Grx1 being a better reducing system for ribonucleotide reductase, as measured by k_{cat}/K_m [43].

Conclusion

Here we show that when the electrochemistry of thioredoxins from archaea is directly probed, both the high and low potential thioredoxins behave similarly. Our Pourbaix diagrams show slopes of -60 mV/pH around neutral pH suggesting the solution-based pK_a values are not accurate representations of the proton coupled electron transfer event. These results call into question the validity of the previously proposed pK_a control model and show it is not a good fit for these archaeal thioredoxins. Additionally, however, we show that the protein fold and stability of the oxidized and reduced forms of the protein can predict whether a redox potential will be oxidizing or reducing.

Supporting Information

S1 Fig. Sequence alignment of *E. coli* Trx1, *T. acidophilum* Trx and *A. fulgidus* Trx1 and Trx3 using sequences deposited at NCBI and Clustal 2.1 for the alignment. Additional Cys residues are highlighted in teal.
(PDF)

S1 Methods. Additional fitting routines for pKa fitting routines and folding/unfolding experiments.
(PDF)

S1 Table. List of mutagenesis primers used to make *Archaeoglobus fulgidus* Trx3 mutants.
(PDF)

S2 Table. Data collection and refinement statistics for *AfTrx3HP*. [a]Values in parentheses are the highest resolution shell. [b]$R_{sym} = \Sigma_{hkl}\Sigma_i |I_i(hkl)\text{-}<I(hkl)>|/\Sigma_{hkl}\Sigma_i I_i(hkl)$, where $I_i(hkl)$ is the ith measured diffraction intensity and $<I(hkl)>$ is the mean intensity for the reflection with the miller index (hkl). [c]$R_{work} = \Sigma_{hkl}||F_o(hkl)|\text{-}|F_c(hkl)||/\Sigma_{hkl}|F_o(hkl)|$. [d]$R_{free} = R_{work}$ for 5% of reflections omitted from refinement. [e]asu, asymmetric unit. [f]RMS, root mean square.
(PDF)

Author Contributions

Conceived and designed the experiments: KDB MD REB SM SEC CLD SJE. Performed the experiments: KDB MD SM SEC. Analyzed the data: KDB MD REB SEC. Contributed reagents/materials/analysis tools: KDB MD SM SEC. Wrote the paper: KDB MD REB CLD SJE.

References

1. Holmgren A. Thioredoxin. Ann Rev Biochem. 1985; 54: 237–271. PMID: 3896121

2. Hiniker A, Bardwell JCA. Disulfide bond isomerization in prokaryotes. Biochemistry. 2003; 42: 1179–1185. PMID: 12564920

3. Chobot SE, Hernandez HH, Drennan CL, Elliott SJ. Direct electrochemical characterization of archaeal thioredoxins. Angew Chem Intl Ed. 2007; 119: 4223–4225.

4. Chivers PT, Prehoda KE, Raines RT. The CXXC Motif: A rheostat in the active site. Biochemistry. 1997; 36: 4061–4066. PMID: 9099998

5. Wunderlich M, Glockshuber R. Redox properties of protein disulfide isomerase (DsbA) from *Escherichia coli*. Protein Sci. 1993; 2: 717–726. PMID: 8495194

6. Wunderlich M, Jaenicke R, Glockshuber R. The redox properties of protein disulfide isomerase (DsbA) of *Escherichia coli* result from a tense conformation of its oxidized form. J Mol Biol. 1993; 233: 559–566. PMID: 8411164

7. Zapun A, Bardwell JCA, Creighton TE. The reactive and destabilizing disulfide bond of DsbA, a protein required for protein disulfide bond formation in vivo. Biochemistry. 1993; 32: 5083–5092. PMID: 8494885

8. Aslund F, Berndt KD, Holmgren A. Redox potentials of glutaredoxins and other thiol-disulfide oxidoreductases of the thioredoxin superfamily determined by direct protein-protein redox equilibria. J Biol Chem. 1997; 272: 30780–30786. PMID: 9388218

9. Lundström J, Holmgren A. Determination of the reduction-oxidation potential of the thioredoxin-like domains of protein disulfide-isomerase from the equilibrium with glutathione and thioredoxin. Biochemistry. 1993; 32: 6649–6655. PMID: 8329391

10. Hawkins HC, de Nardi M, Freedman RB. Redox properties and cross-linking of the dithiol/disulphide active sites of mammalian protein disulphide-isomerase. Biochem J. 1991; 275: 341–340. PMID: 2025221

11. Krause G, Lundström J, Barea JL, Pueyo de la Cuesta C, Holmgren A. Mimicking the active site of protein disulfide-isomerase by substitution of proline 34 in *Escherichia coli* thioredoxin. J Biol Chem. 1991; 266: 9494–9500. PMID: 2033048

12. Holmgren A. Thioredoxin and glutaredoxin systems. J Biol Chem. 1989; 264: 13963–13966. PMID: 2668278

13. Mössner E, Huber-Wunderlich M, Glockshuber R. Characterization of *Escherichia coli* thioredoxin variants mimicking the active-sites of other thiol/disulfide oxidoreductases. Protein Sci. 1998; 7: 1233–1244. PMID: 9605329

14. Lin T-Y, Kim PS. Urea dependence of thiol-disulfide equilibria in thioredoxin: confirmation of the linkage relationship and a sensitive assay for structure. Biochemistry. 1989; 28: 5282–5287. PMID: 2669972

15. Grauschopf U, Winther JR, Korber P, Zander T, Dallinger P, Bardwell JCA. Why is DsbA such an oxidizing disulfide catalyst? Cell. 1995; 83: 947–955. PMID: 8521518

16. Nelson JW, Creighton TE. Reactivity and ionization of the active site cysteine residues of DsbA, a protein required for disulfide bond formation in vivo. Biochemistry. 1994; 33: 5974–5983. PMID: 8180227

17. Guddat LW, Bardwell JCA, Martin JL. Crystal structures of reduced and oxidized DsbA: investigation of domain motion and thiolate stabilization. Structure. 1998; 6: 757–767. PMID: 9655827

18. Darby N, Creighton TE. Characterization of the active site cysteine residues of the thioredoxin-like domains of protein disulfide isomerase. Biochemistry. 1995; 34: 16770–16780. PMID: 8527452

19. Dawson RMC, Elliott DC, Elliott WH, Jones KM. Data for Biochemical Research: Oxford University Press; 1989.

20. Clark WM. Oxidation-Reduction Potentials of Organic Systems. Baltimore: The Williams & Wilkins Company; 1960.

21. Takahashi N, Creighton TE. On the reactivity and ionization of the active site cysteine residues of *Escherichia coli* thioredoxin. Biochemistry. 1996; 35: 8342–8353. PMID: 8679592

22. Jacobi A, Huber-Wunderlich M, Hennecke J, Glockshuber R. Elimination of all charged residues in the vicinity of the active-site helix of the disulfide oxidoreductase DsbA. J Biol Chem. 1997; 272: 21692–21699. PMID: 9268296

23. Heras B, Kurz M, Jarrott R, Shouldice SR, Frei P, Robin G, et al. *Staphylococcus aureus* DsbA does not have a destabilizing disulfide. J Biol Chem. 2008; 283: 4261–4271. PMID: 18077463

24. Dyson HJ, Gippert GP, Case DA, Holmgren A, Wright PE. Three-dimensional solution structure of the reduced form of *Escherichia coli* thioredoxin determined by nuclear magnetic resonance spectroscopy. Biochemistry. 1990; 29: 4129–4136. PMID: 2193685

25. Hamill MJ, Chobot SE, Hernandez HH, Drennan CL, Elliott SJ. Direct electrochemical analyses of a thermophilic thioredoxin reductase: interplay between conformational change and redox chemistry. Biochemistry. 2008; 47: 9738–9746. doi: 10.1021/bi800676g PMID: 18717594

26. Fourmond V, Hoke K, Heering HA, Baffert C, Leroux F, Bertrand P, et al. SOAS: A free program to analyze electrochemical data and other one-dimensional signals. Bioelectrochemistry. 2009; 76: 141–147. doi: 10.1016/j.bioelechem.2009.02.010 PMID: 19328046

27. Lewin A, Crow A, Oubrie A, Le Brun NE. Molecular basis for specificity of the extracytoplasmic thiore-doxin ResA. J Biol Chem. 2006; 281: 35467–35477. PMID: 16971393

28. Lewin A, Crow A, Hodson CTC, Hederstedt L, Le Brun NE. Effects of substitutions in the CXXC active-site motif of the extracytoplasmic thioredoxin ResA. Biochem J. 2008; 414: 81–91. doi: 10.1042/BJ20080356 PMID: 18422485

29. Otwinowski Z, Minor W. Processing of X-ray diffraction data collected in oscillation mode. Methods Enzymol. 1997; 276: 307–326.

30. McCoy AJ, Grosse-Kunstleve RW, Adams PD, Winn MD, Storoni LC, Read RJ. Phaser crystallographic software. J Appl Cryst. 2007; 40: 658–674.

31. Emsley P, Lohkamp B, Scott WG, Cowtan K. Features and development of Coot. Acta Crystallogr Sect D-Biol Crystallogr. 2010; 66: 486–501.

32. Murshudov GN, Vagin AA, Dodson EJ. Refinement of Macromolecular Structures by the Maximum-Likelihood method. Acta Crystallogr Sect D. 1997; 53: 240–255.

33. Project CC. The CCP4 suite: programs for protein crystallography. Acta Crystallogr Sect D. 1994; 50: 760–763.

34. Brunger AT, Adams PD, Clore GM, DeLano WL, Gros P, Grosse-Kunstleve RW, et al. Crystallography & NMR system: A new software suite for macromolecular structure determination. Acta Crystallogr Sect D-Biol Crystallogr. 1998; 54: 905–921.

35. Adams PD, Afonine PV, Bunkoczi G, Chen VB, Davis IW, Echols N, et al. PHENIX: a comprehensive Python-based system for macromolecular structure solution. Acta Crystallogr Sect D-Biol Crystallogr. 2010; 66: 213–221.

36. Laskowski RA, Macarthur MW, Moss DS, Thornton JM. PROCHECK—A Program to Check the Stereo-chemical Quality of Protein Structures. J Appl Cryst. 1993; 26: 283–291.

37. Slaby I, Cerna V, Jeng M-F, Dyson HJ, Holmgren A. Replacement of Trp in Escherichia coli thioredoxin by site-directed mutagenesis affects thermodynamic stability but not function. J Biol Chem. 1996; 271: 3091–3096. PMID: 8621706

38. Holmgren A. Tryptophan fluorescence study of conformational transitions of the oxidized and reduced form of thioredoxin. J Biol Chem. 1972; 247: 1992–1998. PMID: 4552684

39. Pace CN (1986) [14]Determination and analysis of urea and guanidine hydrochloride denaturation curves. Methods Enzymol: Academic Press. pp. 266–280. PMID: 3773761

40. Santoro MM, Bolen DW. Unfolding free energy changes determined by the linear extrapolation method. 1. Unfolding of phenylmethanesulfonyl. alpha.-chymotrypsin using different denaturants. Biochemistry. 1988; 27: 8063–8068. PMID: 3233195

41. Rost J, Rapoport S. Reduction-potential of glutathione. Nature. 1964; 201: 185–185. PMID: 14118272

42. Nordstrand K, Aslund F, Meunier S, Holmgren A, Otting G, Berndt KD. Direct NMR observation of the Cys-14 thiol proton of reduced Escherichia coli glutaredoxin-3 supports the presence of an active site thiol-thiolate hydrogen bond. FEBS Lett. 1999; 449: 196–200. PMID: 10338131

43. Zahedi Avval F, Holmgren A. Molecular mechanisms of thioredoxin and glutaredoxin as hydrogen do-nors for Mammalian s phase ribonucleotide reductase. J Biol Chem. 2009; 284: 8233–8240. doi: 10.1074/jbc.M809338200 PMID: 19176520